Maximizing paraffin to olefin ratio employing simulated nitrogen-rich syngas via Fischer-Tropsch process over Co_3O_4/SiO_2 catalysts

Mahmoudi, Hamid; Jahangiri, Hessam; Doustdar, Omid; Akbari, Nazanin; Wood, Joe; Tsolakis, Athanasios; Wyszynski, Miroslaw Lech

DOI:
10.1016/j.fuproc.2020.106477

Document Version
Peer reviewed version

Citation for published version (Harvard):
Mahmoudi, H, Jahangiri, H, Doustdar, O, Akbari, N, Wood, J, Tsolakis, A & Wyszynski, ML 2020, 'Maximizing paraffin to olefin ratio employing simulated nitrogen-rich syngas via Fischer-Tropsch process over Co_3O_4/SiO_2 catalysts', *Fuel Processing Technology*, vol. 208, 106477. https://doi.org/10.1016/j.fuproc.2020.106477

Maximizing paraffin to olefin ratio employing simulated nitrogen-rich syngas via Fischer-Tropsch process over Co_3O_4/SiO_2 catalysts

Hamid Mahmoudi[a], Hessam Jahangiri[b], Omid Doustdar[a], Nazanin Akbari[a], Joe Wood[c], Athanasios Tsolakis[a], Miroslaw Lech Wyszynski[a,*]

[a] Department of Mechanical Engineering, School of Engineering, University of Birmingham, Birmingham, B15 2TT, UK;
[b] School of Water, Energy and Environment, Cranfield University, Cranfield, MK43 0AL, UK;
[c] School of Chemical Engineering, University of Birmingham, Birmingham, B15 2TT, UK;
*Corresponding author: Email address: m.l.wyszynski@bham.ac.uk (M.L.Wyszynski)

ABSTRACT

The optimization of cobalt oxide (Co_3O_4) loading on silica for the low-temperature Fischer-Tropsch (LTFT) synthesis process employing simulated nitrogen-rich syngas (50 vol%) to produce highly paraffinic biodiesel is studied. Four different amounts of Co_3O_4 varying from 15 to 36 wt% were loaded on silica in order to examine the catalytic performance of Co/SiO_2 catalysts. The supported catalysts were characterized by using XRF, nitrogen physisorption, XRD, TPR, DRIFT and SEM fixed with EDS analysis. The performances of the catalysts were examined in a single channel fixed bed reactor employing simulated nitrogen-rich syngas ($CO:H_2:N_2$ = 17:33:50 vol%). The reactor was operated at P = 20 bar, T = 237 °C and WHSV = 3.0 Nl/h.g_{cat}. The active site concentration was maximized by (i) utilizing all the available surface area of the sphere's porous support, (ii) using ethanolic impregnation solution to hinder sintering of Co_3O_4 phases due to presence of ethoxyl groups, (iii) connecting oxide crystallites to the neighbouring pores by increasing the active metal content. As a result, the production of heavy hydrocarbons per unit of time was maximized with 36 wt% cobalt loading on silica (CO conversion and C_{5+} selectivity were 87.65 and 81.78 mol%, respectively, and also paraffin:olefin ratio was 98:2).

Keywords: Fischer-Tropsch synthesis; cobalt catalyst; silica support; biodiesel; paraffin.

Abbreviations: DRIFT, Diffuse Reflectance Infrared Fourier Transform; EDS, Energy-Dispersive Spectroscopy; FTS, Fischer-Tropsch Synthesis; FWHM, Full-Width Half Maximum; GC-MS, Gas Chromatogram-Mass Spectrometry; JCPDS, Joint Committee on Powder Diffraction Standards; LTFT, Low-Temperature Fischer-Tropsch; PDF, Powder Diffraction File; PPF, Process Path Flow; SEM, Scanning Electron Microscopy; TCD, Thermal Conductivity Detector; TPR, Temperature-Programmed Reduction; WGS, Water Gas Shift; XRD, X-Ray Diffraction; XRF, X-Ray Fluorescence.

1. INTRODUCTION

Biomass-derived hydrocarbon fuels have received attention as alternative fuel sources due to the increase in demand for fossil fuels and concerns regarding climate change [1]. Thermochemical conversion of biomass can be performed by combustion, pyrolysis and gasification [2, 3]. Gasification is one of the commercial approaches to convert biomass into syngas which contains hydrogen (H_2) and carbon monoxide (CO) [3]. In 1922 Han Fischer and Franz Tropsch developed a heterogeneously catalyzed process (Fischer-Tropsch synthesis (FTS)) for the transformation of syngas into different hydrocarbon fractions (lower olefins, gasoline, diesel fuels). Nature of the supporting materials and active metal dispersion are two significant parameters affecting catalyst activity and product selectivity in the FTS process [4]. Supported catalysts are the most preferred to synthesize long-chain hydrocarbons due to the high dispersion of active agents over the support's surface, as well as, the higher thermo-stability degree which extends the catalyst's lifetime [5]. Among certain transition metals employed for FTS catalyzing, cobalt-based catalysts are the most preferred to synthesize middle-distillate hydrocarbons [6]. Higher activity at low temperature (CO conversion per pass), heavy hydrocarbon productivity, higher chain growth probability, higher selectivity to paraffin, lower compounds oxygenating in secondary reactions, lower water gas shift (WGS) reaction and a longer lifetime of cobalt compared to iron catalysts makes it more appropriate to be employed to synthesize diesel fuel and wax [7]. The interaction of active cobalt site with the supporting materials was the subject of various studies, due to its significant catalytic properties [8, 9]. Silica high surface area, high porosity degree, as well as, weaker metal support interaction compared to alumina and titania makes the silica as appropriate support for FTS [10, 11]. Moreover, silica possesses high thermo-stability due to its high Tamman temperature [12].

Cobalt ions are highly diffused into the support lattice when active metal is loaded in a lower amount. The diffusion of cobalt could be obstructed by application of promoters such as Re [13]. The increase in the supported active phase enhances the reducibility of silica-supported Co_3O_4 catalyst [14]. The hydrothermal stability of the catalyst is improved when cobalt oxide species interacted strongly to the oxygen atoms of silanol groups in the silica matrix [15]. Khodakov et al. [9] concluded that the catalytic performance of a narrow pore sized catalyst was better than that of a large pore size due to higher dispersion of the active site over this support. Ma et al. [16] observed that the decrease in the average cobalt cluster diameter by about 30% (from 38.4 nm for a catalyst containing 15 wt% metal content to 27 nm for a catalyst containing 25 wt% metal content) in a cobalt catalyst supported by silica, resulted in an increase in the intrinsic reaction rate constant due to the rise in the density of active Co^0 on the surface site.

Many works of literature are studied about the effect of catalyst types, active metals and supports in FTS process employing nitrogen-free syngas [1, 10, 11]. However, it was not possible to identify in the literature any work which concentrated on the production of highly paraffinic middle distillate fuel using a fixed bed reactor with nitrogen-rich syngas at the maximized conversion rate. The nitrogen-rich syngas is more likely to be used in industry and reduces the cost of biofuel production using syngas derived from air gasification of biomass waste [17]. It is reported that the nitrogen gas concentration is 47.77 ± 1.30 vol% on a dry basis for downdraft fixed bed gasifier [18, 19]. Therefore, all experiments were done using nitrogen-rich syngas (50 vol%) in this study. In order to maximize the conversion of the reactants per pass, a series of four cobalt-based catalysts were prepared in house by employing different concentrations of active metal (cobalt loading: 15, 22, 29 and 35 wt%) over the silica support. The aim of this investigation was to design, build and commission a compact biofuel generator via FTS process eventually

on the scale suitable for an individual farmer or small village to convert their biomass (agricultural waste) into the consumable drop-in liquid fuel. Commercial-scale biofuel plants raise the cost of fuel synthesizing in many aspects. Lowering the capital and operating cost for a mobile biofuel generator will counteract various limitation existing for platform mounted biomass to liquid (BTL) plants [20]. The International Energy Agency (IEA) reported that high production costs and the need for large-scale production facilities are two significant barriers in the utilization of commercial-scale second-generation biodiesel (SGB) in rural areas [21]. Therefore, a miniaturized unit of biofuel generator can be inexpensive and transportable and could deliver ultra-clean drop-in liquid fuel for individual users or small villages. The objectives of this study were as follows:

I. Engineering a heterogeneous catalytic reaction system capable of synthesizing nitrogen-rich syngas in a miniaturized single fixed bed reactor in FTS process.
II. Designing active cobalt/silica catalyst to maximize the conversion rate of syngas to prevent recycling of unreacted raw syngas in downstream and thus minimizing the drop-in liquid production's time for individual users or farmer.
III. Optimization study to achieve high conversion in single pass operation along with high selectivity to long-chain hydrocarbons with maximized paraffin to olefin ratio.

In this research, catalysts performance were tested in a single channel fixed bed reactor employing simulated nitrogen-rich syngas ($CO:H_2:N_2$ = 17:33:50 vol%).

2. EXPERIMENTAL

2.1 Catalyst Preparation

The cobalt catalysts were prepared by one step incipient wetness impregnation of silica support (Fuji Silysia Chemical Ltd., grade: CARiACT Q-10) with different molar ethanolic solutions of cobalt (II) nitrate hexahydrate ($Co(NO_3)_2.6H_2O$, grade: ACS reagent, ≥98%, Sigma Aldrich Co). Before the impregnation, the support was pre-treated by drying in air at 200 °C for 14 h and was followed by calcination at 500 °C for 2 h in an oven [22]. These actions were resulted in complete removal of the physically adsorbed multilayer of water as well as maximizing the concentration of isolated single and geminal OH groups over amorphous silica surface. After impregnation, the catalyst was dried in air at 200 °C for 14 h and then calcined at 500 °C for 4 h to generate the active site phases. The resulting materials were named SUP-Q-10 (silica support) and CAT-Q-X, where X is the amount of cobalt loadings.

2.2 Catalyst Characterization

A wavelength-dispersive XRF (WDXRF) spectrometer (Bruker ® S8 Tiger) combined with an X-ray source (end-window 4-kW Rh X-ray tube) operated at 60 kV, 50 mA (Co) and 30 kV. 100 mA (Si) was employed to perform the quantitative and qualitative analyzing of different elements in the samples using an optimized analyzer crystal (Co: LiF 200 crystal and Si: PET crystal). All operations were performed under a helium atmosphere with a flow rate of 0.7 l/min. For each experiment, a powder sample of 0.4 g was weighed and poured into the sample cup covered with transparent film (Chemplex ®, Mylar: 2.5 μm thin and 63.5 mm diameter). Then the sample cup was mounted in the small mask (8 mm).

The nitrogen physisorption analyses were measured at -195.76 °C utilizing a Micromeritrics ® ASAP 2010 instrument. For each experiment, 1.1 g of each sample was outgassed for 4 h at 90 °C. The surface area of the samples was determined by employing the Brunauer–Emmett–Teller (BET) method. The relative pressure was increased from 0.05769 to 0.9864 to form the multilayer of physically adsorbed nitrogen on the porous structure. Barrett, Joyner, and Halenda (BJH) method was employed to calculate the total pore volume. The relative pressure was decreased to about 0.1168 to evaporate the condensed nitrogen. Kevin equation was used to calculate the core radius [23].

The crystalline phases of the unreduced/calcined catalysts were studied using X-ray diffraction (XRD) method (EQUINOX 3000 motorization-free diffraction system) with monochromatized radiation of Cu-Kα operating at room temperature. The scans (2θ) ranged from 0° to 115° and the samples were analyzed in their original powder form. Metal phases were assigned by comparing the obtained diffraction patterns with those in the standard XRD powder diffraction File (PDF), combined with the Joint Committee on Powder Diffraction Standards (JCPDS). Scherrer equation (Equation 1) was employed to calculate the diameter of Co_3O_4 crystallites using (3 1 1) peaks at 2θ = 36.65° [24, 25].

$$d = \frac{k.\lambda}{\beta.\cos\theta} \times \frac{180^\circ}{\pi} \quad (1)$$

Where d is the mean crystallite diameter (nm), λ the X-ray wavelength (1.54056 Å), and β is the full-width half-maximum (FWHM) of the Co_3O_4 diffraction peak. A k factor of 0.89 was used in the Scherrer equation. The average Co_3O_4 crystallite size ($d(Co_3O_4)$) was converted to the corresponding mean cobalt metal diameter by considering relative molar volumes of cobalt crystallites (Equation 2). Then in Equation 3, the related cobalt

metal dispersion ($D(Co^0)$) was calculated according to the average Co^0 crystallite size ($d(Co^0)$) [24, 25].

$$d(Co^0) = 0.75 \cdot d(Co_3O_4) \quad (2)$$

$$D(Co^0) = \frac{96}{d_{Co^0}} \quad (3)$$

The reduction behaviour of the catalysts was investigated by employing hydrogen temperature-programmed reduction (TPR) using Micromeritics. For each experiment, 0.1 g of calcined sample was loaded in quartz U-shape tube reactor. The sample was purged by flushing nitrogen for 60 minutes, heated from ambient temperature to 150 °C and then cooled to 50 °C. Afterwards, pure hydrogen was introduced to the sample with a total flow rate of 500 cm^3/min. While hydrogen was flowing, the sample's temperature was raised from 50 °C to 900 °C with a ramping rate of 4 °C /min. An on-line thermal conductivity detector (TCD) was utilized to measure the amount of hydrogen gas before and after passing through the sample.

The nature of the acid sites of the catalyst samples was distinguished by employing diffuse reflectance infrared Fourier transform spectroscopy (DRIFTS) of chemisorbed pyridine using Nicolet Avatar 370 MCT. The spectra of the samples were obtained in the wavenumber ranging between 650 – 4000 cm^{-1}. For each experiment, 50 mg of powder samples were diluted with 450 mg of KBr powder (potassium bromide). After that, the samples were loaded into the environmental cell and dried at 50 °C under vacuum conditions. The pyridine was exposed to the samples Ex-situ using a desiccator. Before sample loading in the environmental cell, they were subjected to a vacuum oven to remove the excess physisorbed pyridine.

The scanning electron microscopy (SEM) (Jeol ® JSM 6060)-energy dispersive spectroscopy (EDS) (Oxford instrument Inca 300) surface analysis was performed to evaluate the heterogeneity of the particle size as well as metal repartition over the surface of various catalysts (working distance: 10 mm, signal: SED). The structure of the cobalt catalysts was considered at nano-scale by using FEI strata ® XP 235 dual-beam SEM. The surface mapping on the user defined area was obtained for all of the samples (accelerating voltage 20 kV, live time 140 to 150 seconds, working distance 10 mm and spot size 71).

2.3 FTS Experiment

Figure 1 indicates the schematic diagram of the mini scale biofuel generator along with the Process Path Flow (PPF), designed and developed to convert simulated synthesis gas into long-chain hydrocarbons. The FT hydrogenation reaction was carried out in a tubular mini-structured downdraft fixed bed reactor (seamless stainless steel, 19 mm inner diameter, 1.65 mm wall thickness, and 530 mm length). The reactor was mounted in a tube furnace with the temperature ranging from 40 to 1100 °C to provide the heat zone. To achieve a uniform wall temperature, a metal jacket inside the furnace tube surrounded the reactor. For each experiment, 2 g of the catalyst was diluted with silicon carbide (mesh particle size 200-450, Sigma Aldrich Co.) with a mass ratio of 1:12 and then were loaded into the reactor [26]. The diluted catalyst was packed with glass beads (3 mm diameter) and glass wool (Sigma Aldrich Co.). A thermocouple was positioned along the centreline of the reactor to monitor the bed temperature during the reaction. A simulated nitrogen-rich syngas bottle was used to provide feedstock for the FT activity ($CO:H_2:N_2$ = 17:33:50 vol%). A calibrated smart mass flow controller was employed to regulate the volumetric flow rate of the syngas (Bronkhorst Ltd).

Before the FT reaction, the catalytic bed was purged using nitrogen gas for 120 minutes at 140 °C. The reduction process started with flowing hydrogen gas (pure hydrogen, zero grade, BOC Co.) over the catalyst starting at 60 °C. While the hydrogen gas was flowing, the bed temperature was increased linearly with time to 200 °C and held at this step for 60 minutes. Then the temperature was ramped up to 340 °C and held for 60 minutes. The final temperature ramping was targeted to 450 °C, and the cobalt catalyst was left at this temperature for 14 h with a volumetric hydrogen flow rate of 3.0 Nl/h. The gas velocity was kept high to prevent the cobalt catalyst sintering by removing the produced water from the reduction reaction. After finishing the reduction step, the reactor temperature was lowered to 170 °C, and the syngas was introduced to the catalyst. Subsequently, the pressure was increased to the desired pressure, and the bed temperature was increased to the required reaction temperature. The catalyst was put on stream for 12 h to determine CO conversion, methane (CH_4) and carbon dioxide (CO_2) selectivity, and products' selectivity over this period of reaction time.

Two liquid/gas separators were used to separate the liquid products from the gaseous stream. Liquid hydrocarbon products were collected in a cold trap, cooled externally at 10 °C using a counter-current heat exchanger. Changes in the concentration of carbon monoxide and produced carbon dioxide were monitored on-line by using a modified AVL Digas™ 440 every 30 to 90 minutes. A flame-ionized detector was used on-line to analyze the hydrocarbons from C_1 to C_8 using pora plot Q column to separate the products combined with a gas chromatogram (GC). 250 µL of the sample injected into the GC using helium as the carrier gas. The initial oven temperature was adjusted at 5 °C, while the temperature was ramped up at 7.5 °C/min to reach 225 °C and then held for 8 minutes. The detector temperature was set at 320 °C. Quantitative analysis was carried out to measure the concentration of different compounds in a sample of the gas. In regards to

heavy hydrocarbons, the product distribution was analyzed offline employing a DB1 column combined with gas chromatography-mass spectrometry (GC-MS).

As several simultaneous chemical reactions take place in the FT regime, producing both desired and undesired products, Equations 4 to 7 were employed to analyze the gaseous products. Equation 4 was defined to demonstrate the fraction of reactant that has been consumed and Equations 5 to 7 were employed to show the portion of reactants that have been converted to valuable and valueless products.

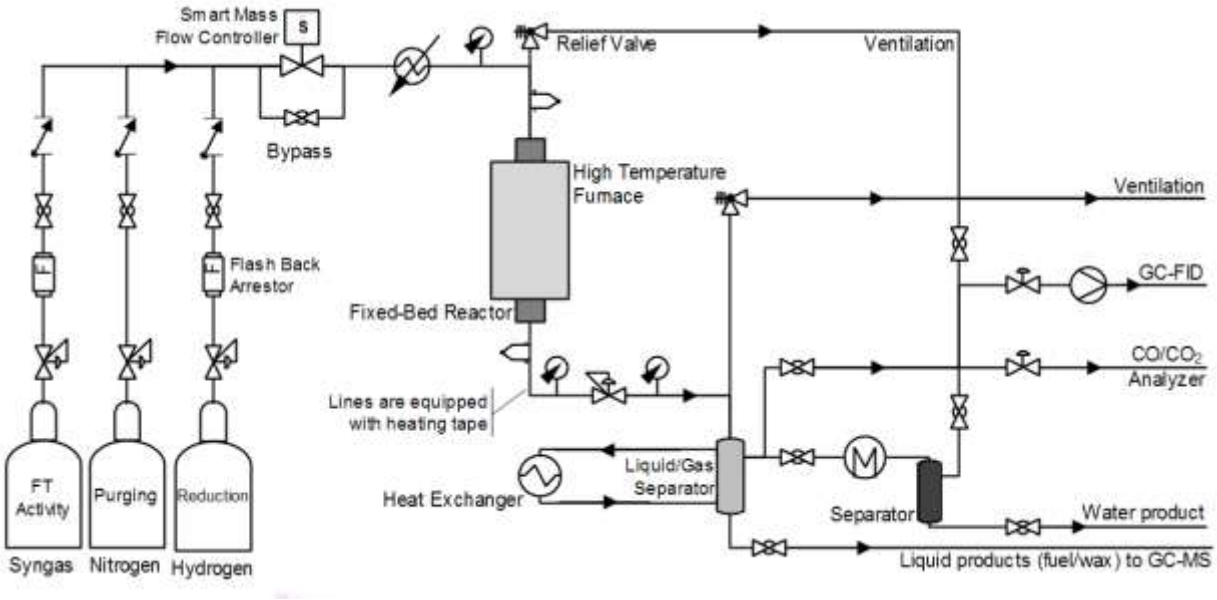

Figure 1. Schematic diagram of small scale biodiesel generator via Fischer-Tropsch Synthesis (FTS) process and utilized equipment along with Process Path Flow (PPF).

$$X_{CO}\ (CO\ Conversion\ \%) = \frac{moles\ of\ inlet\ CO - moles\ of\ outlet\ CO}{moles\ of\ inlet\ CO} \times 100 \qquad (4)$$

$$S_{CO_2}\ (CO_2\ selectivity\ \%) = \frac{moles\ of\ CO_2\ produced}{moles\ of\ inlet\ CO - moles\ of\ outlet\ CO} \times 100 \qquad (5)$$

241 $C_x\ selectivity\ \%\ (x = 1 - 4)$

242 $$= \frac{moles\ of\ C_x\ produced}{(moles\ of\ CO_{in} - moles\ of\ \ CO_{out}) - moles\ of\ CO_{2_{produced}}} \times 100 \quad (6)$$

243 $$S_{5^+} = 100 - S_{C_1} - S_{C_2} - S_{C_3} - S_{C_4} \quad (7)$$

244

245

246

247

248

249

250

251

252

253

254

255

256

257

258

259

260

261

3. RESULTS AND DISCUSSION

3.1 X-Ray Fluorescence (XRF) Elemental Analysis

The quantitative elemental analyses of the prepared catalysts were carried out by using a wavelength dispersive XRF spectrometer. **Table 1** shows cobalt content on silica. The metal concentrations over the support's surface were controlled by changing the molarity of the cobalt impregnation solutions. The XRF analysis confirms that increasing the molarity of impregnation solutions leads to higher loading of cobalt over the silica support.

3.2 Nitrogen Adsorption/Desorption Analysis

The N_2 adsorption isotherms are displayed in **Figure 2**. All isotherms showed exhibit hysteresis and belonged to type IV isotherms [27]. The results of the surface area measurements, as well as the pore volume and pore diameter, are represented in **Table 1**. The results show that the BET surface area of the silica support (SUP-Q-10) was decreased after the impregnation of the cobalt catalyst. The loading of the active metal over the porous support resulted in the blockage of some pores and subsequently, a reduction in specific surface areas [28]. Hereafter, the surface areas of CAT-Q-15, CAT-Q-22 and CAT-Q-29 did not change significantly. However, there is a drop in the surface area for the highest Co loading (CAT-Q-36) which might be attributed to more plugging of the pores of support by the active metal species, which led to inaccessible pores during the nitrogen adsorption [29]. The increase of Co species did not change the average pore diameter, while BJH analysis of the isotherms revealed that the pore volumes continuously decreased as the Co loading was increased. These results suggest the silica surface is near to saturation at 15 wt% and that as the Co loading is increased crystallite growth continues unabated in the porous structure. It is reported that the pore volume

and diameter of Co/silica remained unchanged with increasing the cobalt loading and this can be attributed to the impact of aqueous impregnation on mesoporous structures or additional heat treatments during the preparation process [30, 31].

Table 1. XRF elemental analysis and textural characteristics of porous silica support and different supported cobalt catalysts measured by nitrogen physisorption technique.

Sample	Co (%)	BET surface area (m^2/g)	Average pore diameter (nm)	Pore volume (cm^3/g)
SUP-Q-10	0	277.4	17.2	1.20
CAT-Q-15	15.4	247.9	17.4	1.08
CAT-Q-22	22.0	249.7	16.7	1.04
CAT-Q-29	29.3	250.8	16.2	1.01
CAT-Q-36	35.7	225.9	16.4	0.92

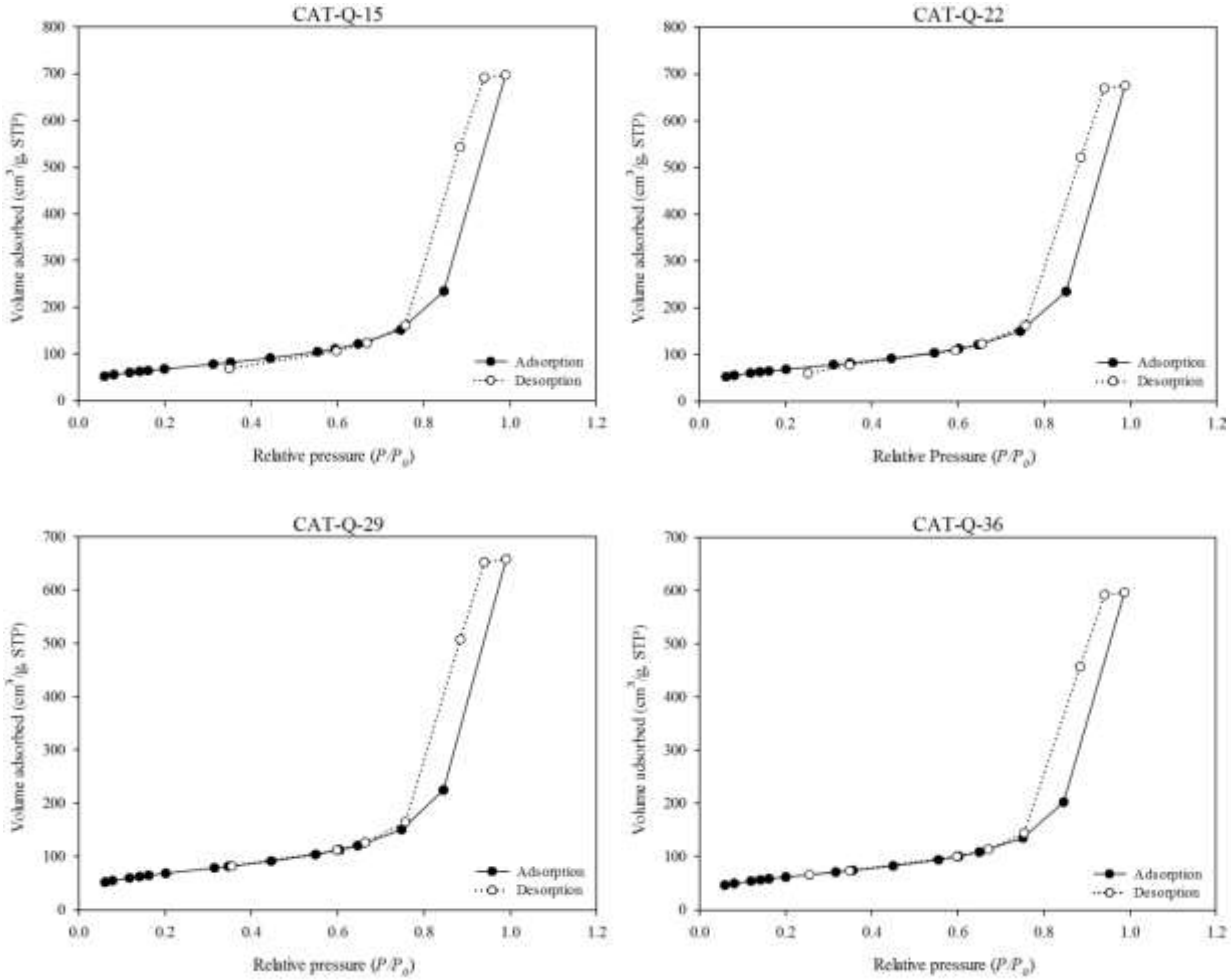

293

294 **Figure 2.** Nitrogen adsorption (filled circle) and desorption (empty circle) for different

295 supported cobalt catalysts.

296

297

298

299

300

301

302

303

304

305

3.3 X-Ray Diffraction (XRD) Analysis

The crystalline structure of the cobalt supported samples was analyzed by XRD analysis (**Figure 3)**. The presence of Co_3O_4 spinal phases with 2θ values of 36.65°, 38.21°, 44.74° and 65.13° were observed in all of the diffractograms [32]. The intensity of our results is different from some literature [24, 30]. However, some other studies reported that the intensity of cobalt/silica catalysts could change which is associated with catalysts preparation methods and calcination temperature [33, 34]. The Co_3O_4 is the most dominant phase when the cobalt nitrate is decomposed under air [34]. The wide diffraction peaks are illustrated that the signal at 36.65° are changing with increasing the cobalt loading, due to the presence of a small Co_3O_4 crystalline phase formed over porous silica support. It is reported that the metallic cobalt crystallite size is proportional to the size of the Co_3O_4 crystalline phase [24]. In addition to the cobalt cluster size, the average size of supported Co_3O_4 crystallites is greatly influenced by the porous silica support's structure [9, 35]. **Table 2** listed the average crystallite size of Co_3O_4 (according to the Scherrer equation based on the characteristic diffraction peak at 2θ = 36.65°), the cobalt metal particle diameter (Equation 2) as well as the metal dispersion (Equation 3). It is observed that Co_3O_4 crystallite size of CAT-Q-15 decreased with further cobalt loading (up to 29 wt%). However, the average crystallite size of the Co_3O_4 phase was increased by 19% from 12.98 nm (CAT-Q-29) to 16.04 nm (CAT-Q-36), containing the highest cobalt concentration. CAT-Q-29 sample assigns the highest estimated cobalt dispersion among the others. In some cases (CAT-Q-15 and CAT-Q-22), the crystallite sizes calculated from the XRD measurements are larger than the pore diameter of the catalysts. This could be suggested by the highly branched structure of the silica supports, which able the cobalt

metals to be formed and interconnected to other neighbouring pores and to be placed on the exterior surface of the supports [30, 36].

Table 2. Average Co_3O_4 crystallite size estimated Co^0 particle diameter and estimated cobalt dispersion for different supported cobalt catalysts.

Sample	Co_3O_4 crystallite diameter (nm)	Estimated Co^0 particle diameter (nm)	Estimated cobalt dispersion (%)
CAT-Q-15	24.79	18.59	3.87
CAT-Q-22	19.47	14.60	4.93
CAT-Q-29	12.98	9.73	7.39
CAT-Q-36	16.04	12.03	5.98

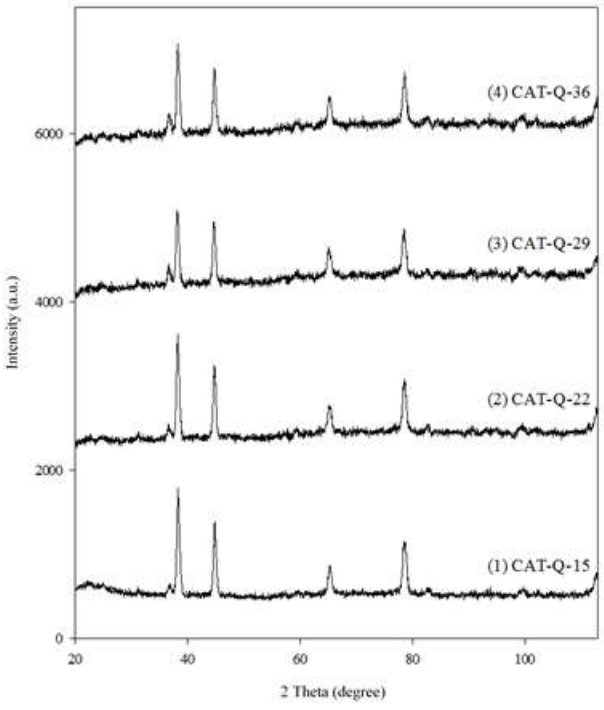

Figure 3. XRD diffraction spectrogram of different calcined and unreduced catalysts.

3.4 Temperature-Programmed Reduction (TPR) Analysis

TPR has been conducted to determine the temperature at which Co_3O_4 is reduced to elemental cobalt, thereby identifying the interaction species and operating temperature of the Fisher-Tropsch reactor. **Figure 4** shows the TPR profiles of all catalysts, when reduced under H_2, as a function of temperature. The TPR experiments show there are several reduction events occurring. The two TPR peaks occur between 250 °C and 640 °C, and the final reduction event happens above 750 °C. The first two events are ascribed to the sequential reduction of Co_3O_4 to CoO and finally to elemental Co (Equations 8 and 9 respectively) [37-40].

$$Trivalent\ reduction: \quad Co_3O_4 + H_2 \rightarrow 3CoO + H_2O \tag{8}$$

$$Divalent\ reduction: \quad 3CoO + 3H_2 \rightarrow 3Co^0 + 3H_2O \tag{9}$$

Co_3O_4 reduction to the CoO is ascribed to the low-temperature reduction peaks (CAT-Q-15: 368 °C, CAT-Q-22: 337 °C, CAT-Q-29: 335 °C, CAT-Q-36: 345 °C) for the four differently loaded cobalt catalysts. On the other hand, the reductions which occurred at 450, 440, 475 and 455 °C are ascribed to the reduction of CoO to the free metallic Co^0 in CAT-Q-15, CAT-Q-22, CAT-Q-29 and CAT-Q-36 respectively [37-40]. The reductions of all of the catalysts were completed below 480 °C. As shown in the figure, all of the catalysts display a broad peak at temperatures higher than 750 °C (CAT-Q-15: 770 °C, CAT-Q-22: 804 °C, CAT-Q-29: 760 °C, CAT-Q-36: 758 °C), which could be attributed to the reduction of surface cobalt interacting with surface silicates [41, 42] or alternatively to the cobalt fraction contained in the inner cavities of the silica support [43]. The low-temperature peak observed in some TPR spectra is attributed to the reduction of residual cobalt nitrate [33]. Overall, a slight temperature shift in the TPR profiles to the low temperature

is observed from 15 wt% to 29 wt % cobalt loading, and the acid strength decreased. Therefore, CAT-Q-29 appeared to be more easily reduced in comparison with CAT-Q-15 and CAT-Q-22. This trend in the reduction profile of the catalysts is in agreement with the literature [10, 44]. However, the bulk reduction of cobalt oxide is slightly shifted to a higher temperature in the CAT-Q-36. This might be attributed to either the exact nature of the cobalt or the formation of cobalt silicate compounds [10]. Furthermore, increasing the cobalt loading on silica increased the H_2 consumption area and thus could show a higher reduction degree of Co_3O_4 to metallic Co [25, 44]. Qualitatively, it is evident that CAT-Q-22 is reduced at the lowest temperature of 440 °C and CAT-Q-29 at the highest temperature of 475 °C. Therefore, the reactor must be brought to at least 475 °C in order to reduce the catalyst to the active Co/SiO_2 form.

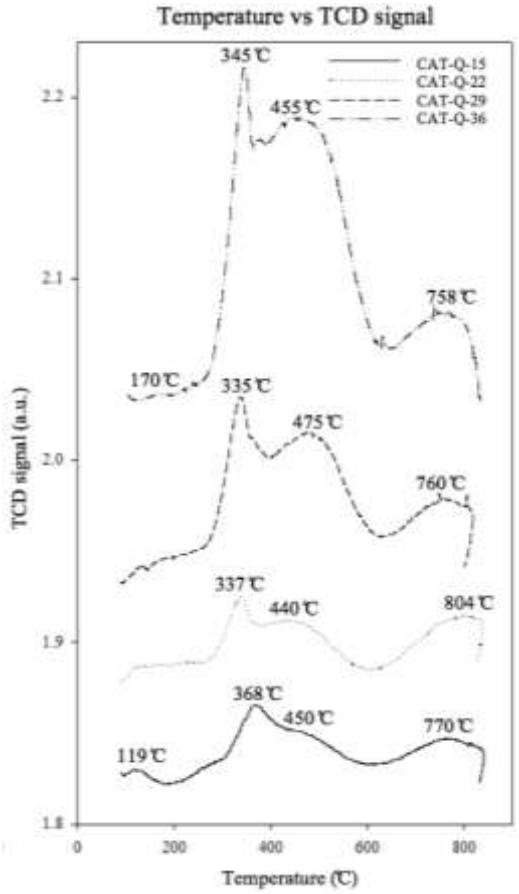

Figure 4. TPR profiles for different supported cobalt catalysts.

3.5 Pyridine Adsorption/DRIFTS

Pyridine adsorption, followed by DRIFTS explored the nature of acid sites. Application of pyridine that interacts with the sites varying in acidity enables determination of Lewis and Brønsted acid sites in the samples [45]. Spectra of probe molecule interacting with pre-calcined oxide catalysts are shown in **Figure 5**. Lewis acid sites are indicated through the adsorption mode at 1440 and 1620 cm^{-1}, whereas Brønsted acid sites showed adsorption modes at 1550 cm^{-1} [45]. The results indicated that different cobalt loadings on silica have mainly Lewis acid species and a small amount of Brønsted acid species [46].

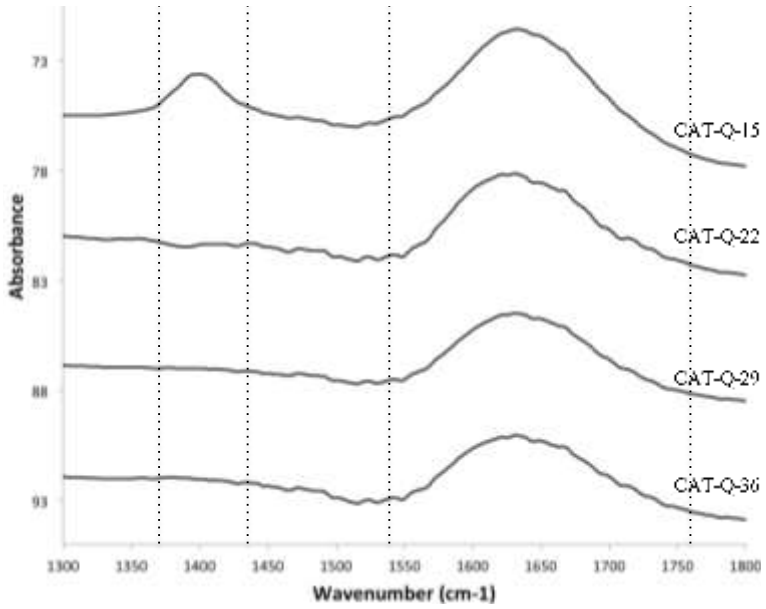

Figure 5. DRIFT spectra of pyridine adsorbed on different supported cobalt catalysts.

3.6 Microstructural and Morphological Structure

Heterogeneity of particle size, as well as repartition of active sites over the surface of different catalysts, were considered by employing the SEM instrument (**Figure 6-9**). In addition to the morphology of the catalysts, typical microanalysis of the surface was investigated by EDS. The concentration of cobalt particles is demonstrated in the white colour, while the dark colour illustrates the silica support surface. Composition maps of CAT-Q-15 and CAT-Q-22 obtained from SEM-EDS analysis illustrated the homogeneous dispersion of cobalt over the entire analyzed spot area. CAT Q-15 showed less dense and better homogeneous morphology than CAT-Q-22. It could be noticed that better active site distributions were achieved in these two catalysts compared to those of high cobalt content samples (CAT-Q-29 and CAT-Q-36). The cobalt particles over the surface of CAT-Q-29 and CAT-Q-36 catalysts might be agglomerated and exhibited non-uniform distribution due to thermal gradient. As a result of the thermal gradient, an outward flow from inside to the outside of the pores of support occurred, and subsequently, the metal oxides were concentrated on the support surface, particularly when the metal content was increased, which leads to more accumulation of metal oxide and inhomogeneous formation of lumps [47]. The typical SEM imagining of the samples along with EDS mapping illustrates that the cobalt particles are distributed on the external surface of the support granule in powder catalysts [48]. The poly-dispersed spherical metal particles were observed for all catalysts [49].

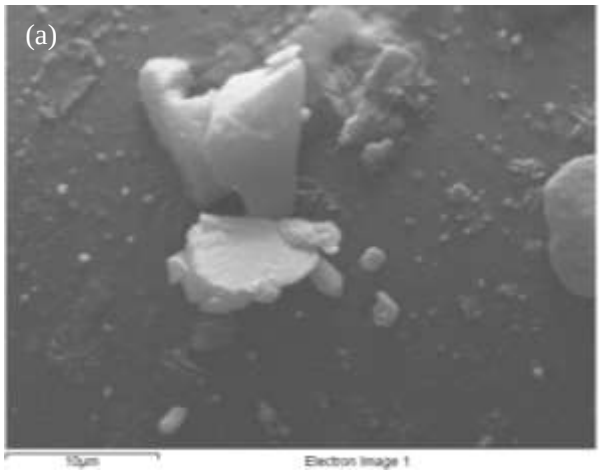

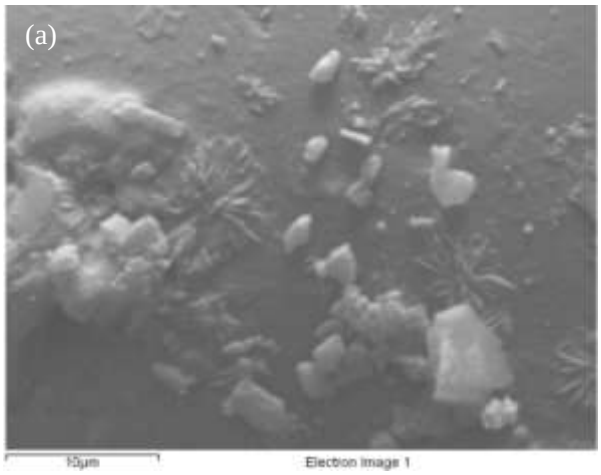

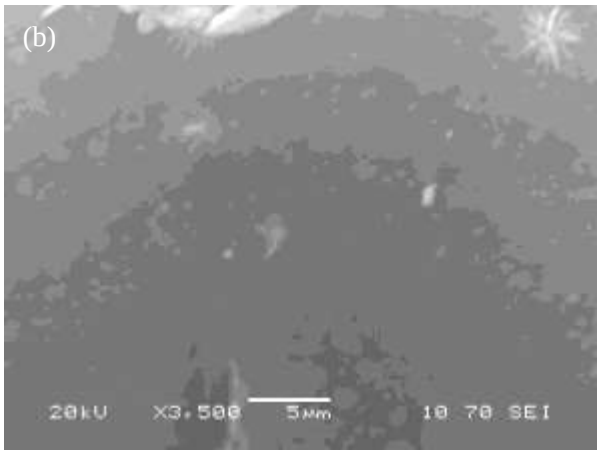

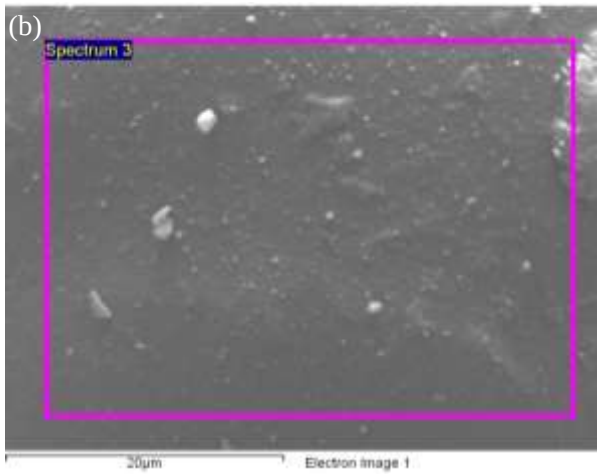

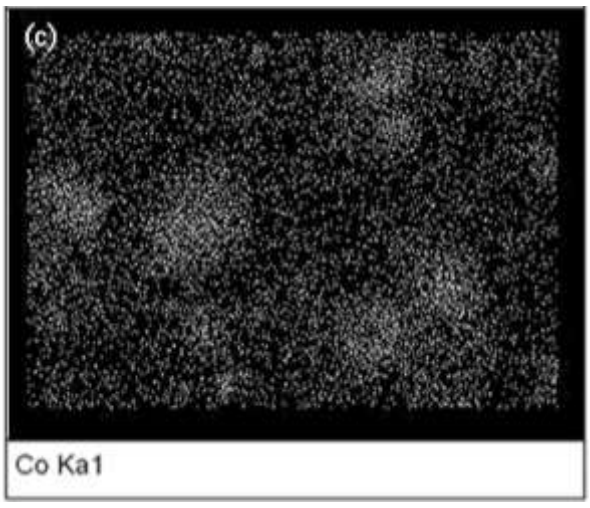

413

414 **Figure 6.** SEM micrographs (Figures 6.a and 6.b) and EDX micro-analysis (Figure
415 6.c) of sample CAT-Q-15.

Figure 7. SEM micrographs (Figures 7.a and 7.b) and EDX micro-analysis (Figure 7.c) of sample CAT-Q-22.

416

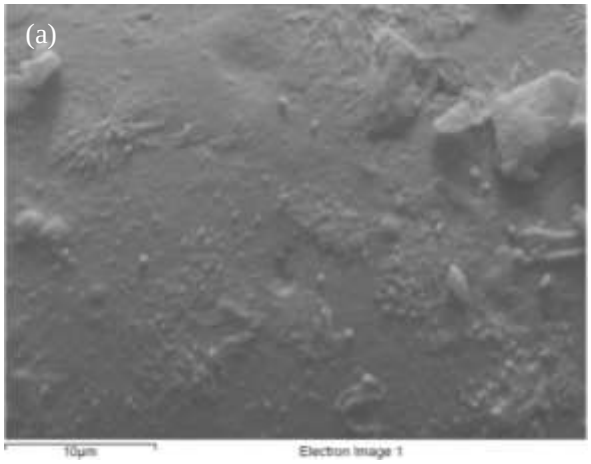

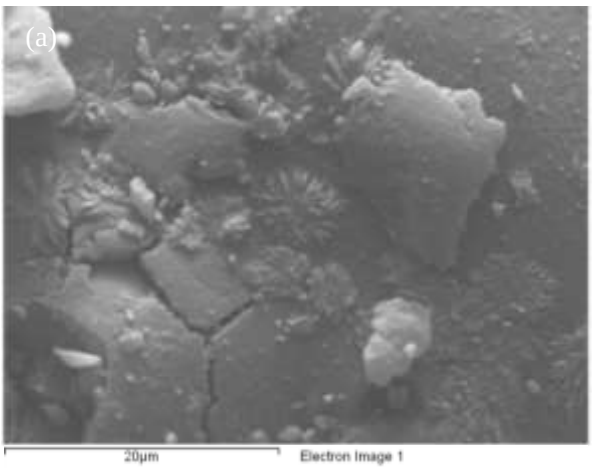

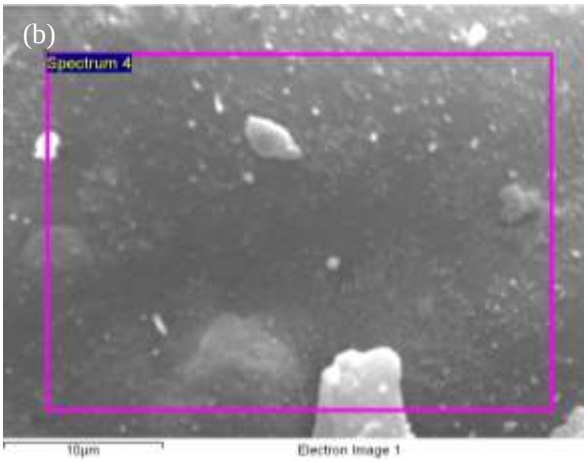

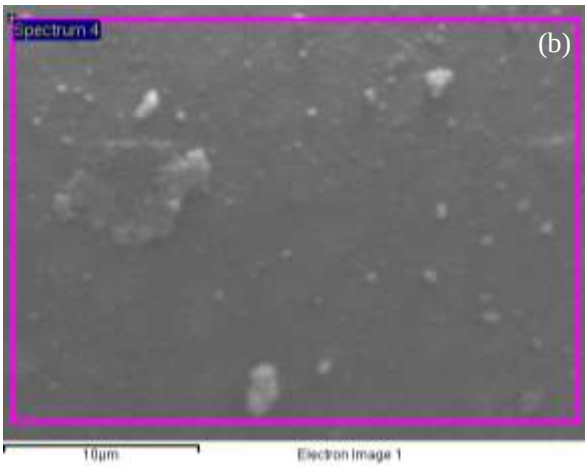

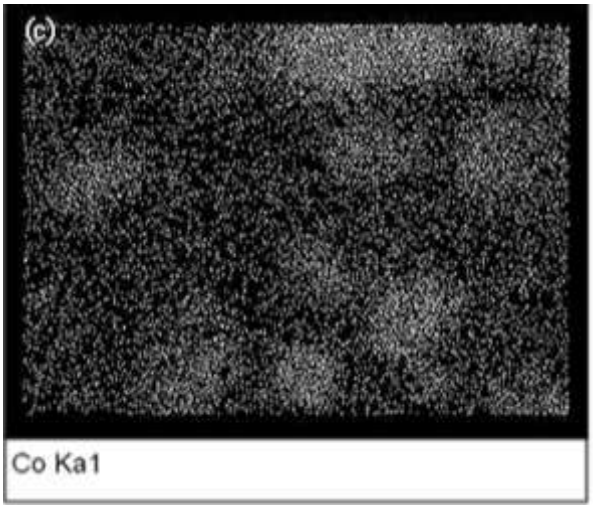

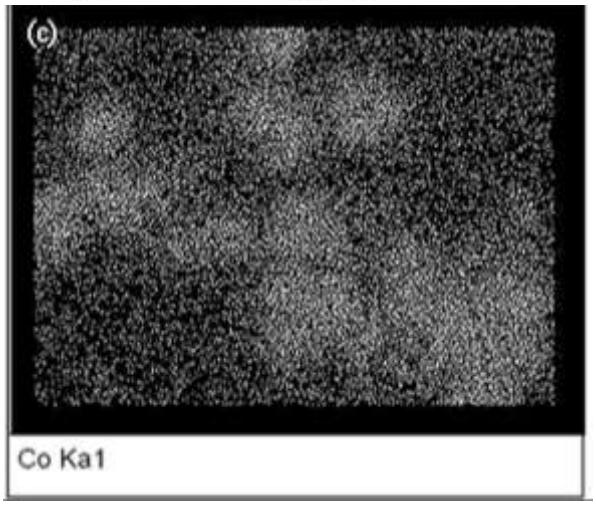

417

418 **Figure 8.** SEM micrographs (Figures 8.a and 8.b) and EDX micro-analysis (Figure
419 8.c) of sample CAT-Q-29.

Figure 9. SEM micrographs (Figures 9.a and 9.b) and EDX micro-analysis (Figure 9.c) of sample CAT-Q-36.

420

421

3.7 Catalyst Activity and Selectivity in the FTS Process

The FT performances of the different catalysts were considered at 237 °C, 20 bar and 3.0 Nl/h.g_{cat} WHSV. The hydrogenation activities of all catalysts were examined in the same reactor set-up and reaction conditions, as well as the gaseous environment, to ensure the comparison was correctly made. The catalyst activities in terms of CO conversion as well as hydrocarbon/by-product selectivity were reported for 12 h in **Table 3**. As the cobalt content increased from 15 to 36 wt%, the hydrogenation activity of the catalyst in terms of carbon monoxide conversion was increased by 68.4% (from 27.67 to 87.65 mol%). The results are in good agreement with those reported by Sun et al. [50].

The increase in CO conversion is associated with the higher active sites of cobalt species in CAT-Q-36. The increase in the concentration of active metal sites resulted in a highly active supported cobalt catalyst due to higher reducibility. It is reported that FTS activity correlated with higher Co_3O_4 reduction [25, 44]. In the TPR profile (Figure 4), much higher H_2 consumption could be illustrated the observed larger area for the Co_3O_4 reduction on the sample CAT-Q-36 and could demonstrate the highest reducibility. Furthermore, the Co_3O_4 reduction area decreased with reducing the cobalt loading and thus could decline the catalyst reducibility [25, 44].

The activity of the cobalt catalyst is proportional to the concentration of accessible surface metallic cobalt (Co^0). The high hydrogenation activity of CAT-Q-36 compared to low cobalt content catalysts confirms that the cobalt particles have not been aggregated due to the increase in cobalt loading. However, Medina et al. [51] observed that CO conversion decreased with the increasing of the metal content above 20 wt%.

The product distributions of the catalysts were affected mainly by the amount of metal loading. All of the catalysts showed relatively high selectivity in methane formation. The

increases in the concentration of active sites resulted in a decrease in the production of methane. The maximum CH_4 selectivity was reported for the CAT-Q-15 (S_{CH4} = 41.85 mol%), and the minimum selectivity of methane was for CAT-Q-36 (S_{CH4} = 13.44 mol%). It is generally assumed that methane hydrocarbon is favoured when CO and intermediates are weakly adsorbed by active sites [34]. In contrast to the methane formation, water gas shift (WGS) reaction showed a different trend. CAT-Q-15 showed the lowest carbon dioxide production, whereas an increase in the metal content increased the CO_2 selectivity.

CAT-Q-36 revealed the highest selectivity in C_{5+} hydrocarbon (S_{C5+} = 81.78 mol%) compared to the others, while CAT-Q-15 was allocated the lowest selectivity in heavy hydrocarbons production (S_{C5+} = 38.82 mol%). It is reported that the Lewis acid sites of Co-based catalysts in FTS improved the CO adsorption and dissociation and thus increasing C_{5+} selectivity [52, 53]. We also observed that Lewis acid sites are identified as the active species (Figure 5), and thus they were responsible for the C_{5+} hydrocarbons production in FTS process.

It is also reported that small cobalt crystallites formed long-chain hydrocarbons [51]. The presence of strained siloxane bridges over dehydroxylated silica surface, which react with ethanol, increase the density of ethoxyl groups (Si – O – C_2H_5). The ethoxyl groups interfere with the sintering of Co_3O_4 during the endothermic decomposition of cobalt nitrate. These phenomena result in the synthesis of active cobalt-based catalyst, uniform repartition of active phase as well as the formation of smaller cobalt crystallite size over support surface [54].

This investigation confirms that the conversion per pass of reactants could be maximized by increasing the concentration of the active sites over the support surface without any

dramatic reduction in the accessibility of the Co^0 particles. Furthermore, the pore blockage of the silica support was almost absent. This investigation was successful in increasing the selectivity to diesel fraction in liquid products with maximized paraffin:olefin ratio (98:2) using fixed-bed reactor technology. However, future catalysts selectivity tests at the same activity as well as maximizing paraffin to olefin ratio for low cobalt loading are required to be studied.

Table 3. Catalytic performances of the different supported cobalt catalysts in FTS (CO conversion (X_{CO}), products selectivity (S_{CO2}, S_{CH4}, S_{C2-C4}, S_{C5+}) and reaction conditions: 237 °C, 20 bar and 3.0 Nl/h.g_{cat} WHSV).

Catalyst	$X_{(CO)}$ (mol%)	The selectivity of gas-phase products (mol%)					
		$S_{(CO2)}$	$S_{(CH4)}$	$S_{(C2)}$	$S_{(C3)}$	$S_{(C4)}$	$S_{(C5+)}$
CAT-Q-15	27.67	1.96	41.85	4.07	8.10	7.16	38.82
CAT-Q-22	44.95	2.09	28.00	2.68	5.19	4.53	59.60
CAT-Q-29	61.74	2.88	24.09	0.21	0.39	0.36	74.95
CAT-Q-36	87.65	5.32	13.44	1.10	1.90	1.78	81.78

Experimental data for CAT-Q-36 at the optimum condition: liquid phase mass fraction (*Wi*), a liquid produced known as LP (ml) and distribution of paraffin and olefin hydrocarbons within diesel fraction (C_{12} – C_{22}).					
	C_7 – C_{11} (wi)		**C_{12} – C_{22} (wi)**	**C_{23+} (wi)**	**LP (ml)**
CAT-Q-36	14.91		81.70	3.39	4.45
	N-paraffin %	**Iso-paraffin %**	**Total paraffin %**	**Total olefin %**	**Alcohol %**
CAT-Q-36	58.95	39.16	98.11	1.10	0.79

3.8 Maximizing Normal Paraffin/Olefin Ratio in FT Synthesis

Paraffin are the most preferred hydrocarbons in the FT synthesis as they are stable compounds due to the absence of the pi bond in their carbon skeleton and are generally unreactive. The produced alkanes from FTS process are mainly straight-chained hydrocarbons. However, the olefins outputs are mostly tertiary [55].

In order to maximize the normal paraffin (N-paraffin), the CAT-Q-36 was selected due to the highest CO conversion (**Table 3**). The product distribution, which is collected at optimum reaction conditions for CAT-Q-36, is shown in **Table 4**. The maximum CO conversion (98.22 mol%) and N-paraffin production (78.32 mol%) were achieved at 245 °C, 25 bar and 3.0 Nl/h.g_{cat} WHSV. When the conversion increased at the optimum reaction condition, the N-paraffin to olefin ratio increased, which is attributed to the secondary reactions (α-olefin readsorption) and changes in termination mechanism [43].

The paraffins are produced through three major routes in FT synthesis. These three routes are termination by hydrogenation of alkyl groups, secondary hydrogenation of α-olefin and readsorption with chain initiation followed by hydrogenation termination [56, 57]. The present investigation increased the termination degree in FT reaction as well as the degree of the secondary reaction, and it could be associated with the partial water pressure for cobalt/silica catalyst [33, 43]. Lowering the partial water pressure in the reaction regime increased the degree of secondary hydrogenations of α-olefin. Controlling the partial water pressure provided more available primary olefins for re-insertion and chain-growth through secondary reaction [43].

Table 4. The fraction of N-paraffin and olefin hydrocarbons in optimized condition for CAT-Q-36 catalyst (reaction conditions: 245 °C, 25 bar and 3.0 Nl/h.g_{cat} WHSV).

Conversion (CO)	98.22 mol%
Selectivity to diesel fraction (C_{12} – C_{22})	81.70 mol%
Type of hydrocarbon in diesel fraction	**Mass fraction (wi)**
Iso-paraffin	18.45
N-paraffin	78.32
Total paraffin	96.77
Olefins	2.04
Alcohols	1.19

To sum up, all experiment conditions demonstrated a stable FT performance, and no catalyst deactivation was observed for 24 hr. However, future extended recycling and the ageing test is required to be investigated. Using the nitrogen-rich syngas (which is more likely to be used in industry from air gasification of biomass waste) and increasing the CO conversation and minimizing the drop-in liquid production's time reduce the cost of compact biofuel generator in several manners (no need for CO recycling, no need for fuel upgrading and reduce the farmer cost). In this study, an effort was made to design and prepare an active Co/SiO_2 catalysts for a cost-efficient LTFT process. Hence, the investigation advanced the research towards (i) designing and engineering highly active cobalt-based catalyst capable of synthesizing nitrogen-rich syngas (50 vol%) in a single fixed bed reactor and (ii) developing active silica-supported cobalt catalyst to maximize the conversion rate of syngas to prevent recycling of unreacted raw syngas in downstream and (iii) optimization study from achieving high conversion with maximized paraffin to olefin ratio.

4. CONCLUSIONS

The study was carried out to examine the effect of metal precursor loading on the catalytic behaviour of the cobalt supported silica powder. The catalytic performance of a powder Co/SiO_2 catalyst was investigated by utilizing fixed-bed reactor technology in a low-temperature Fischer-Tropsch synthesis (LTFT) process operating at 237 °C bed temperature, 20 bar reaction pressure and 3.0 $Nl/h.g_{cat}$ WHSV. The nitrogen-rich syngas was used with a ratio of $CO:H_2:N_2$ = 17:33:50 vol%. The increase in the concentration of active metal sites resulted in a highly active supported cobalt catalyst. The metal loading influenced the cobalt crystallite size and subsequently the cobalt particle size. The conversion of the reactants was maximized by increasing the concentration of active cobalt sites over the large surface area of the silica support. CAT-Q-36 had the highest conversion (87.65 mol%) and selectivity in C_{5+} hydrocarbon (81.78 mol%), but CAT-Q-15 had the lowest conversion (27.67 mol%) and selectivity (38.82) which correlated with the Lewis acid sites of Co-based catalyst. The maximum paraffin:olefin ratio was 98:2 for CAT-Q-36 in the presence of nitrogen-rich syngas (50 vol%) using fixed-bed reactor technology.

ACKNOWLEDGEMENTS

The support of Fuji Silysia Chemical Ltd is highly appreciated and acknowledged by the author for providing qualified catalyst support. Moreover, the author would like to acknowledge Dr Jackie Deans, Mr John Wedderburn, Mr Jeff Sutton, Mrs Theresa Morris and Mr Paul Stanley for their technical support at the University of Birmingham.

REFERENCES

[1] H. Jahangiri, J. Bennett, P. Mahjoubi, K. Wilson, S. Gu, A review of advanced catalyst development for Fischer–Tropsch synthesis of hydrocarbons from biomass derived syn-gas, Catalysis Science & Technology, 4 (2014) 2210-2229.

[2] H.C. Ong, W.-H. Chen, A. Farooq, Y.Y. Gan, K.T. Lee, V. Ashokkumar, Catalytic thermochemical conversion of biomass for biofuel production: A comprehensive review, Renewable and Sustainable Energy Reviews, 113 (2019) 109266.

[3] I. Martínez, V. Kulakova, G. Grasa, R. Murillo, Experimental investigation on sorption enhanced gasification (SEG) of biomass in a fluidized bed reactor for producing a tailored syngas, Fuel, 259 (2020) 116252.

[4] J.L. Hodala, D.J. Moon, K.R. Reddy, C.V. Reddy, T.N. Kumar, M.I. Ahamed, A.V. Raghu, Catalyst design for maximizing C5+ yields during Fischer-Tropsch synthesis, International Journal of Hydrogen Energy, (2020, https://doi.org/10.1016/j.ijhydene.2019.12.021).

[5] A. Saib, M. Claeys, E. Van Steen, Silica supported cobalt Fischer–Tropsch catalysts: effect of pore diameter of support, Catalysis today, 71 (2002) 395-402.

[6] C.G. Okoye-Chine, M. Moyo, X. Liu, D. Hildebrandt, A critical review of the impact of water on cobalt-based catalysts in Fischer-Tropsch synthesis, Fuel Processing Technology, 192 (2019) 105-129.

[7] R. Guettel, U. Kunz, T. Turek, Reactors for Fischer-Tropsch Synthesis, Chemical Engineering & Technology, 31 (2008) 746-754.

[8] S. Sun, K. Fujimoto, Y. Zhang, N. Tsubaki, A highly active and stable Fischer–Tropsch synthesis cobalt/silica catalyst with bimodal cobalt particle distribution, Catalysis Communications, 4 (2003) 361-364.

[9] A.Y. Khodakov, R. Bechara, A. Griboval-Constant, Fischer–Tropsch synthesis over silica supported cobalt catalysts: mesoporous structure versus cobalt surface density, Applied Catalysis A: General, 254 (2003) 273-288.

[10] B.C. Dunn, P. Cole, D. Covington, M.C. Webster, R.J. Pugmire, R.D. Ernst, E.M. Eyring, N. Shah, G.P. Huffman, Silica aerogel supported catalysts for Fischer–Tropsch synthesis, Applied Catalysis A: General, 278 (2005) 233-238.

[11] X. Li, M.U. Nisa, Y. Chen, Z. Li, Co-Based Catalysts Supported on Silica and Carbon Materials: Effect of Support Property on Cobalt Species and Fischer–Tropsch Synthesis Performance, Industrial & Engineering Chemistry Research, 58 (2019) 3459-3467.

[12] S. Qing, X. Hou, L. Li, G. Feng, X. Wang, Z. Gao, W. Fan, Deactivation feature of Cu/SiO2 catalyst in methanol decomposition, International Journal of Hydrogen Energy, 44 (2019) 16667-16674.

[13] E. Yaghoobpour, Y. Zamani, S. Zarrinpashne, A. Zamaniyan, Fischer–Tropsch synthesis: effect of silica on hydrocarbon production over cobalt-based catalysts, Chemical Papers, 73 (2019) 205-214.

[14] E. Yaghoobpour, Y. Zamani, S. Zarrinpashne, A. Zamaniyan, Profound synergetic effect of metal oxide promoters and TiO2–SiO2 binary support in cobalt Fischer-Tropsch catalyst, Journal of the Chinese Chemical Society, (2019) 1-15.

[15] L. Liu, D.K. Wang, D.L. Martens, S. Smart, E. Strounina, J.C. Diniz da Costa, Physicochemical characterisation and hydrothermal stability investigation of cobalt-incorporated silica xerogels, RSC Advances, 4 (2014) 18862-18870.

[16] W. Ma, G. Jacobs, D.E. Sparks, M.K. Gnanamani, V.R.R. Pendyala, C.H. Yen, J.L.S. Klettlinger, T.M. Tomsik, B.H. Davis, Fischer–Tropsch synthesis: Support and cobalt cluster size effects on kinetics over Co/Al2O3 and Co/SiO2 catalysts, Fuel, 90 (2011) 756-765.

[17] R.G.d. Santos, A.C. Alencar, Biomass-derived syngas production via gasification process and its catalytic conversion into fuels by Fischer Tropsch synthesis: A review, International Journal of Hydrogen Energy, (2019, https://doi.org/10.1016/j.ijhydene.2019.07.133).

[18] C.A. Estrada, A. Melgar, J.F. Pérez, Performance prediction of a decentralized power plant (120 kWe) using a multi-particle model of a downdraft biomass gasification process, Energy Conversion and Management, 181 (2019) 258-271.

[19] F.V. Tinaut, A. Melgar, B. Giménez, M. Reyes, Characterization of the combustion of biomass producer gas in a constant volume combustion bomb, Fuel, 89 (2010) 724-731.

[20] K. Sahoo, E. Bilek, R. Bergman, S. Mani, Techno-economic analysis of producing solid biofuels and biochar from forest residues using portable systems, Applied Energy, 235 (2019) 578-590.

[21] A. Eisentraut, Sustainable production of second-generation biofuels: Potential and perspective in major economies and delevloping countries, in, International Energy Agency, OECD/IEA, 2010.

[22] A.Y. Khodakov, W. Chu, P. Fongarland, Advances in the development of novel cobalt Fischer-Tropsch catalysts for synthesis of long-chain hydrocarbons and clean fuels, Chemical Reviews, 107 (2007) 1692-1744.

612 [23] B. Huang, C.H. Bartholomew, B.F. Woodfield, Improved calculations of pore size
613 distribution for relatively large, irregular slit-shaped mesopore structure, Microporous
614 and Mesoporous Materials, 184 (2014) 112-121.

615 [24] C. Chen, H. Yuuda, X. Li, Fischer–Tropsch synthesis over one eggshell-type Co/SiO2
616 catalyst in a slurry phase reactor, Applied Catalysis A: General, 396 (2011) 116-122.

617 [25] Y. Lu, P. Zhou, J. Han, F. Yu, Fischer–Tropsch synthesis of liquid hydrocarbons over
618 mesoporous SBA-15 supported cobalt catalysts, RSC Advances, 5 (2015) 59792-59803.

619 [26] D. van Herk, P. Castaño, M. Quaglia, M.T. Kreutzer, M. Makkee, J.A. Moulijn, Avoiding
620 segregation during the loading of a catalyst–inert powder mixture in a packed micro-bed,
621 Applied Catalysis A: General, 365 (2009) 110-121.

622 [27] K. Sing, Reporting physisorption data for gas/solid systems with special reference to
623 the determination of surface area and porosity (Provisional), Pure and Applied
624 Chemistry, 54 (1982) 2201-2218.

625 [28] M. Trépanier, A. Tavasoli, A.K. Dalai, N. Abatzoglou, Co, Ru and K loadings effects on
626 the activity and selectivity of carbon nanotubes supported cobalt catalyst in Fischer–
627 Tropsch synthesis, Applied Catalysis A: General, 353 (2009) 193-202.

628 [29] G. Prieto, A. Martínez, R. Murciano, M.A. Arribas, Cobalt supported on
629 morphologically tailored SBA-15 mesostructures: The impact of pore length on metal
630 dispersion and catalytic activity in the Fischer–Tropsch synthesis, Applied Catalysis A:
631 General, 367 (2009) 146-156.

632 [30] E. Lira, C.M. López, F. Oropeza, M. Bartolini, J. Alvarez, M. Goldwasser, F.L. Linares, J.-
633 F. Lamonier, M.J. Pérez Zurita, HMS mesoporous silica as cobalt support for the Fischer–
634 Tropsch Synthesis: Pretreatment, cobalt loading and particle size effects, Journal of
635 Molecular Catalysis A: Chemical, 281 (2008) 146-153.

636 [31] A.Y. Khodakov, V.L. Zholobenko, R. Bechara, D. Durand, Impact of aqueous
637 impregnation on the long-range ordering and mesoporous structure of cobalt containing
638 MCM-41 and SBA-15 materials, Microporous and Mesoporous Materials, 79 (2005) 29-
639 39.

640 [32] A.Y. Khodakov, A. Griboval-Constant, R. Bechara, V.L. Zholobenko, Pore size effects
641 in Fischer Tropsch synthesis over cobalt-supported mesoporous silicas, Journal of
642 Catalysis, 206 (2002) 230-241.

643 [33] J.-S. Girardon, A.S. Lermontov, L. Gengembre, P.A. Chernavskii, A. Griboval-Constant,
644 A.Y. Khodakov, Effect of cobalt precursor and pretreatment conditions on the structure
645 and catalytic performance of cobalt silica-supported Fischer–Tropsch catalysts, Journal
646 of Catalysis, 230 (2005) 339-352.

[34] J.-S. Girardon, E. Quinet, A. Griboval-Constant, P. Chernavskii, L. Gengembre, A. Khodakov, Cobalt dispersion, reducibility, and surface sites in promoted silica-supported Fischer–Tropsch catalysts, Journal of Catalysis, 248 (2007) 143-157.

[35] K. Jalama, N.J. Coville, H. Xiong, D. Hildebrandt, D. Glasser, S. Taylor, A. Carley, J.A. Anderson, G.J. Hutchings, A comparison of Au/Co/Al2O3 and Au/Co/SiO2 catalysts in the Fischer–Tropsch reaction, Applied Catalysis A: General, 395 (2011) 1-9.

[36] T. Witoon, M. Chareonpanich, J. Limtrakul, Effect of hierarchical meso-macroporous silica supports on Fischer-Tropsch synthesis using cobalt catalyst, Fuel Processing Technology, 92 (2011) 1498-1505.

[37] A.M. Venezia, V. La Parola, L.F. Liotta, G. Pantaleo, M. Lualdi, M. Boutonnet, S. Järås, Co/SiO2 catalysts for Fischer–Tropsch synthesis; effect of Co loading and support modification by TiO2, Catalysis Today, 197 (2012) 18-23.

[38] A.Y. Khodakov, J. Lynch, D. Bazin, B. Rebours, N. Zanier, B. Moisson, P. Chaumette, Reducibility of Cobalt Species in Silica-Supported Fischer–Tropsch Catalysts, Journal of Catalysis, 168 (1997) 16-25.

[39] A.Y. Khodakov, A. Griboval-Constant, R. Bechara, F. Villain, Pore-size control of cobalt dispersion and reducibility in mesoporous silicas, The Journal of Physical Chemistry B, 105 (2001) 9805-9811.

[40] H. Ming, B.G. Baker, Characterization of cobalt Fischer-Tropsch catalysts I. Unpromoted cobalt-silica gel catalysts, Applied Catalysis A: General, 123 (1995) 23-36.

[41] G. Jacobs, T.K. Das, Y. Zhang, J. Li, G. Racoillet, B.H. Davis, Fischer–Tropsch synthesis: support, loading, and promoter effects on the reducibility of cobalt catalysts, Applied Catalysis A: General, 233 (2002) 263-281.

[42] W.S. Yang, H.W. Xiang, Y.Y. Xu, Y.W. Li, Characteristics and reactivities of cobalt based mesoporous silica catalysts for fischer-tropsch synthesis, in: R.R.W.-S.A.C.W.L. Sang-Eon Park, C. Jong-San (Eds.) Studies in Surface Science and Catalysis, Elsevier, 2003, pp. 693-696.

[43] S. Storsæter, Ø. Borg, E.A. Blekkan, A. Holmen, Study of the effect of water on Fischer–Tropsch synthesis over supported cobalt catalysts, Journal of Catalysis, 231 (2005) 405-419.

[44] Y. Wang, B. Hou, J. Chen, L. Jia, D. Li, Y. Sun, Ethylenediamine modified Co/SiO2 sol–gel catalysts for non-ASF FT synthesis of middle distillates, Catalysis Communications, 10 (2009) 747-752.

[45] F. Hao, J. Zhong, P.-L. Liu, K.-Y. You, H.-A. Luo, Amorphous SiO2–Al2O3 supported Co3O4 and its catalytic properties in cyclohexane nitrosation to ε-caprolactam:

682 Influences of preparation conditions, Journal of Molecular Catalysis A: Chemical, 363–364
683 (2012) 41-48.

684 [46] G. Novodárszki, H.E. Solt, J. Valyon, F. Lónyi, J. Hancsók, D. Deka, R. Tuba, M.R. Mihályi,
685 Selective hydroconversion of levulinic acid to γ-valerolactone or 2-
686 methyltetrahydrofuran over silica-supported cobalt catalysts, Catalysis Science &
687 Technology, 9 (2019) 2291-2304.

688 [47] B.K. Sharma, M.P. Sharma, S. Kumar, S.K. Roy, S.K. Roy, S. Badrinarayanan, S.R.
689 Sainkar, A.B. Mandale, S.K. Date, Studies on cobalt-based Fischer–Tropsch catalyst and
690 characterization using SEM and XPS techniques, Applied Catalysis A: General, 211 (2001)
691 203-211.

692 [48] B. Jongsomjit, T. Wongsalee, P. Praserthdam, Catalytic behaviors of mixed TiO2-SiO2-
693 supported cobalt Fischer–Tropsch catalysts for carbon monoxide hydrogenation,
694 Materials Chemistry and Physics, 97 (2006) 343-350.

695 [49] H. Karaca, P. Fongarland, A. Griboval-Constant, A.Y. Khodakov, K. Hortmann, S. Van
696 Donk, Intergranular and intragranular cobalt repartitions in alumina supported Fischer–
697 Tropsch catalysts promoted with platinum, Comptes Rendus Chimie, 12 (2009) 668-676.

698 [50] S. Sun, N. Tsubaki, K. Fujimoto, The reaction performances and characterization of
699 Fischer–Tropsch synthesis Co/SiO2 catalysts prepared from mixed cobalt salts, Applied
700 Catalysis A: General, 202 (2000) 121-131.

701 [51] C. Medina, R. García, P. Reyes, J.L.G. Fierro, N. Escalona, Fischer Tropsch synthesis
702 from a simulated biosyngas feed over Co(x)/SiO2 catalysts: Effect of Co-loading, Applied
703 Catalysis A: General, 373 (2010) 71-75.

704 [52] G.R. Johnson, A.T. Bell, Effects of Lewis acidity of metal oxide promoters on the
705 activity and selectivity of Co-based Fischer–Tropsch synthesis catalysts, Journal of
706 Catalysis, 338 (2016) 250-264.

707 [53] X. Li, Y. Chen, M.U. Nisa, Z. Li, Combating poison with poison—Irreducible Co2SiO4
708 as a promoter to modify Co-based catalysts in Fischer-Tropsch synthesis, Applied
709 Catalysis B: Environmental, 267 (2020) 118377.

710 [54] A.F. Lucredio, J.D.A. Bellido, A. Zawadzki, E.M. Assaf, Co catalysts supported on SiO2
711 and γ-Al2O3 applied to ethanol steam reforming: Effect of the solvent used in the catalyst
712 preparation method, Fuel, 90 (2011) 1424-1430.

713 [55] X. Wang, M. Economides, Advanced Natural Gas Engineering, Elsevier, 2013.

714 [56] V. Sage, Y. Sun, P. Hazewinkel, T. Bhatelia, L. Braconnier, L. Tang, K. Chiang, M. Batten,
715 N. Burke, Modified product selectivity in Fischer-Tropsch synthesis by catalyst pre-
716 treatment, Fuel Processing Technology, 167 (2017) 183-192.

717 [57] S. Storsæter, D. Chen, A. Holmen, Microkinetic modelling of the formation of C1 and
718 C2 products in the Fischer–Tropsch synthesis over cobalt catalysts, Surface Science, 600
719 (2006) 2051-2063.

720